ACS Macro Letters

pubs.acs.org/macroletters Letter

Modeling Bending and Kinking of DNA Minicircles in Elongational Flow

Richard B. Huang and Patrick S. Doyle*

Cite This: https://doi.org/10.1021/acsmacrolett.6c00246 Read Online

ACCESS | Metrics & More | Article Recommendations | Supporting Information

ABSTRACT: DNA minicircles are a model system for DNA bending mechanics, and their response to nonuniform forcing, such as flow, provides insight into the deformation of broader DNA nanostructures in application environments. In this work we use molecular dynamics simulations to investigate DNA minicircles undergoing deformation and structural transitions in strong elongational flow. We derive an analytical model based on the worm-like chain and the extensional flow potential that predicts the extent of deformation without additional fitting parameters, and show that the data collapse across chain lengths when expressed in terms of the elasto-viscous number. Under uniaxial extensional flow, minicircles adopt a "racetrack" shape, concentrating bending energy toward the extrema of the minicircle along the extensional axis. At large flow strengths, the localized bending disrupts the double helix, resulting in a kink that is predicted by a dimensionless kinking number. DNA minicircles are relevant in biological processes such as gene expression, plasmids, and histone wrapping and, more generally, as building blocks for DNA nanostructures at similar length scales. These results provide a framework for understanding DNA deformation under nonuniform forcing in environments such as nanopores and microfluidic devices.

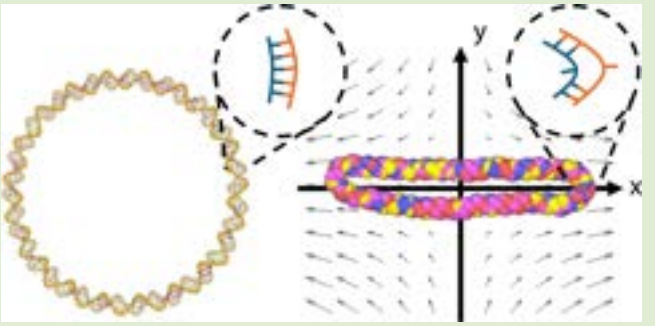

DNA is a ubiquitous natural biopolymer that encodes genetic information as a sequence of nucleotide monomers. Owing to its relatively simple chemical composition and extensive characterization, DNA has also long served as a model system for studying polymer mechanics and single-polymer dynamics.[1] Its mechanical response is important not only in biological settings, but also in synthetic DNA nanostructures, whose stability and functionality depend on how they respond to external forces.[2,3]

In many settings of interest, those forces are hydrodynamic. A concrete example is nanopore-based sensing, where DNA nanostructures are driven through a pore and their precisely defined geometry produces distinct signatures during translocation.[4−6] Structural elements can be linked to signatures, enhancing detection and classification of nanoscale objects such as viral contaminants in medicine.[4] In this setting, a more detailed, mechanistic understanding of how DNA responds to hydrodynamic forcing would enable a robust mapping between structure and measured signature.

Many DNA nanostructures have been characterized mechanically through their response to uniform forcing resulting in an isotension state, such as optical or magnetic tweezers.[3,7] In contrast, hydrodynamic forcing acts along the contour of a polymer, generating position-dependent tension that depends on the chain conformation. This distributed forcing leads to qualitatively different behavior, and in polymer physics has been shown to lead to phenomena such as coil−stretch transitions, molecular individualism, and hysteresis in elongational flow.[8−12] Large, many-kilobase DNA chains have been canonical experimental systems to observe these behaviors. Large circular DNA molecules have been studied in elongational flow and were found to exhibit a shifted coil−stretch transition and less diverse molecular individualism than comparable linear chains.[1,13] In the many-kilobase regime where dynamics can be directly visualized with microscopy, chains are far longer than DNA persistence length and thus strong bending is not relevant.

DNA minicircles are small, cyclized, double-stranded DNA chains with lengths on the order of 100 bp. An example 200 bp DNA minicircle is visualized in Figure 1(a). Because they have persistence-length scales, they are strongly bent, and so are often used to study DNA bending mechanics.[14−16] These mechanics are relevant in understanding many natural cellular processes, including gene expression, plasmids, and histone wrapping for DNA packaging.[15,17] Because minicircles are small, their dynamic response is much less accessible to the

Received: May 1, 2026
Revised: June 26, 2026
Accepted: July 1, 2026

ACS Publications © XXXX American Chemical Society

Downloaded from http://pubs.acs.org/amlccd/article-pdf/doi/10.1021/acsmacrolett.6c00246/6627656/acsmacrolett.6c00246.pdf by MASSACHUSETTS INST OF TECHNOLOGY user on 31 July 2026

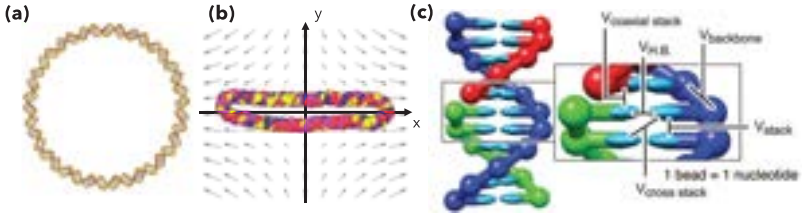

Figure 1. (a) 200 bp DNA minicircle in static conditions visualized in oxView.[28] (b) 200 bp DNA minicircle in uniaxial elongational flow with primary axis of extension in the *x*-direction. The stagnation point is set at the center of mass of the system. Snapshot from OVITO;[29] nucleotide colors indicate base identity: A = red, C = blue, G = yellow, and T = purple. (c) Schematic of the oxDNA model. Hydrogen bonding, backbone connectivity, and several stacking interactions are captured in the model. Reproduced with permission from ref 30. Copyright 2013 American Chemical Society.

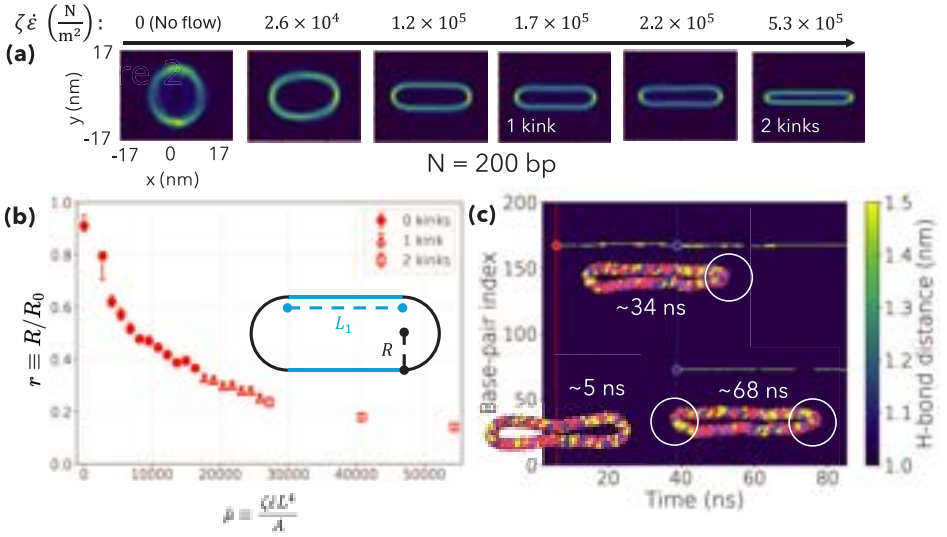

Figure 2. (a) Steady-state 2D heatmaps of 200 bp DNA minicircles under increasing extensional forcing. Using the Stokes drag estimate with $d = 1$ nm and $\mu = 10^{-3}$ Pa·s, the corresponding strain rates are 0, 4.8×10^5, 2.1×10^6, 3.1×10^6, 4.0×10^6, and 9.5×10^6 s^{-1}. (b) Racetrack deformation $r = R/R_0$ plotted against the elasto-viscous number $\bar{\mu}$. Filled circles denote unkinked chains, open triangles one-kink chains, and open squares two-kink chains. Error bars show standard deviations; an example racetrack fit is shown in Figure S1(b). (c) Base-pair distances for a representative 200 bp trajectory at $\zeta\dot{\epsilon} = 5.27 \times 10^5$ N m^{-2}. Base pairs with separation exceeding 1.25 nm are identified as kinked. The snapshot at ~34 ns shows a one-kink conformation, while the snapshot at ~68 ns shows a two-kink conformation.

single-molecule imaging methods used for many-kilobase DNA, leaving hydrodynamic behaviors in this regime comparatively unexplored.

In this Letter, we use molecular dynamics simulations to investigate the deformation and structural transitions that DNA minicircles undergo in uniaxial elongational flow. We use uniaxial elongational flow as it is a canonical linear flow with a uniform velocity gradient and an associated velocity potential, allowing a study of polymer dynamics isolated from rotational effects. The extensional flow field is illustrated in Figure 1(b). We find that minicircles deform into a racetrack-like shape that concentrates curvature toward their extrema along the extensional axis, and use this observation together with worm-like chain bending energy and the flow potential to develop an analytical model for the unkinked response. The model predicts deformation without additional fitting parameters and collapses the data across chain lengths through the elasto-viscous number. At stronger flow forcing, curvature localization disrupts the double helix and induces kinking, revealing a distinct dimensionless group governing the onset of kinking in flow.

Many models exist for simulating DNA. For our purposes, oxDNA strikes a balance between capturing nucleotide-level details while enabling the simulation of longer time and spatial scales without extensive computational resources.[18,19] A schematic of the oxDNA model is shown in Figure 1(c). The smallest units captured by the model are the backbone and base of each nucleotide. The model includes hydrogen bonding, backbone connectivity, excluded-volume interactions, Debye−Hückel electrostatics for salt-screened interactions, stacking between neighboring bases on the same strand, cross-stacking between bases on opposite strands, and coaxial stacking between bases at helix−helix interfaces, such as across nicks or between adjacent duplex ends.[19,20] The simulations are freely draining, with solvent treated implicitly through Langevin dynamics and hydrodynamic interactions not included. Hydrodynamic interactions are expected to be most important for longer, coiled polymers. For the shorter, extended minicircles studied here, they may change effective drag prefactors but are not expected to alter the qualitative deformation behavior. The oxDNA model has been used extensively to study strongly bent DNA, including DNA minicircles, at equilibrium.[16,21] It has also previously been applied to study force-driven DNA dynamics such as overstretching, duplex rupture, DNA-origami mechanics, and nanopore transport.[22−26] We use the implementation of the oxDNA2 model in LAMMPS.[27]

https://doi.org/10.1021/acsmacrolett.6c00246
ACS Macro Lett. XXXX, XXX, XXX−XXX

Downloaded from http://pubs.acs.org/amlccd/article-pdf/doi/10.1021/acsmacrolett.6c00246/6276756/acsmacrolett.6c00246.pdf by MASSACHUSETTS INST OF TECHNOLOGY user on 31 July 2026

DNA minicircles were generated as circles of N base pairs, equilibrated in static conditions in native oxDNA, and then simulated in LAMMPS at 300 K with a Langevin thermostat and 0.1 M monovalent salt. Uniaxial extensional flow was applied implicitly as a position-dependent force on each nucleotide corresponding to the quadratic potential $U_{ext} = -\frac{1}{2}\zeta_{disc}\dot{\epsilon}\left[(x - x_{COM})^2 - \frac{1}{2}(y - y_{COM})^2 - \frac{1}{2}(z - z_{COM})^2\right]$. Here, ζ_{disc} is the drag coefficient associated with a single nucleotide bead. Using a Stokes drag estimate, $\zeta_{disc} = 3\pi\mu d$, where $d = 1$ nm is the bead diameter and $\mu = 0.001$ Pa·s is the solvent viscosity. We further denote a distinct ζ as the drag coefficient per unit contour length of DNA. The two are related by $\zeta = \frac{2}{a}\zeta_{disc}$, where $a = 0.34$ nm is the contour length per base pair, and the factor of 2 accounts for the two nucleotides in each base pair. In the simulations, the product $\zeta_{disc}\dot{\epsilon}$ is prescribed directly as a single quantity measuring flow forcing, rather than by specifying $\dot{\epsilon}$ and ζ_{disc} separately. The physical strain rates reported below are then obtained by back-calculating $\dot{\epsilon}$ from this imposed quantity using the Stokes' drag estimate for ζ_{disc}.

DNA minicircles with $N = 200$ bp were simulated at increasing extensional forcing and projected onto 2D space to generate the steady-state heatmaps shown in Figure 2(a); details of the heatmap construction are given in the Supporting Information. As the forcing increases, the minicircles deform from an approximately circular shape toward a racetrack-like conformation, with curvature concentrated toward each minicircle's extrema along the extensional axis and the rest of the contour becoming relatively straight. The rightmost heatmap corresponds to $\zeta\dot{\epsilon} = 5.27 \times 10^5$ N m^{-2}, which maps to a strain rate of $\dot{\epsilon} = 9.5 \times 10^6$ s^{-1}.

To quantify this deformation, we model the steady-state shape as a racetrack with semicircular caps of radius R connected by linear segments of length L_1, so that the total contour length is $L = aN = 2\pi R + 2L_1$. For each steady-state conformation, we determine the racetrack of equal contour length that best fits the heatmap points and define the deformation measure $r \equiv R/R_0$, where $R_0 = aN/(2\pi)$ is the radius of the undeformed minicircle. We then plot r against the elasto-viscous number $\bar{\mu} \equiv \frac{\zeta\dot{\epsilon}L^4}{A}$, which compares viscous forcing to bending stiffness and is commonly used for elastic filaments in viscous flows.[31,32] Here, $A = k_B T l_p$ is the DNA bending stiffness, with persistence length $l_p = 50$ nm. As shown in Figure 2(b), r decreases monotonically with increasing $\bar{\mu}$, indicating progressively stronger flattening of the minicircle and sharper cap curvature under flow. This decrease becomes more gradual as $\bar{\mu}$ increases, but near $\bar{\mu} \approx 1.6 \times 10^4$ it no longer appears to level off. The resulting change in trend suggests that an additional structural response sets in around this range.

The bending mechanics of DNA chains longer than persistence length have been shown to follow the well-known Kratky–Porod worm-like chain (WLC) model.[33,34] Canonical experiments by Cloutier and Widom observed sharply looped DNA in protein–DNA complexes with far higher flexibility than that predicted by WLC.[35] Since then, many experiments and simulations with minicircles and other setups have also observed this increase in flexibility.[16,17,36−40] This strong bending is known to be caused by the formation of kinks in the backbone of the DNA double helix.[15] Kinks may form via disrupting the hydrogen bonding in the base pair or disrupting stacking interactions but maintaining the base pair, with experimental evidence for both mechanisms.[15,17,37−39,41] By concentrating curvature in the caps of the racetrack shape, local bending appears to become strong enough to induce kinking. The local transition enables the whole chain to adopt a racetrack shape with lower r, lowering overall energy. Prior studies that have used oxDNA to investigate strongly bent DNA have defined kinking with structural and energetic definitions.[16,21] We focus on the structure, and thus define kink formation as bending-induced base-pair melting. Strong elongational flow concentrates curvature toward the minicircle's extrema along the extensional axis, resulting in high bending stresses that break the hydrogen bonding of one or more base pairs locally, enabling the macroscopic shape of the minicircle to change. In Figure 2(a) and (b) the appearance of kinks is noted. In Figure 2(c), the distance between nucleotides in each base pair is tracked over time for one 200 bp minicircle at $\zeta\dot{\epsilon} = 5.27 \times 10^5$ N m^{-2}. Early in the trial, after steady state but prior to kinking, deformation is present but the high-curvature regions are not yet sharp. After a kink forms around bp 160, one extremum has much sharper curvature. After two kinks form, the system has entered its steady-state shape where both high-curvature regions are sharper. It is possible for base pairs to come back together and reform hydrogen bonds, though this becomes less likely for higher strain rates.

We analyze the minicircle deformation by considering the energies. We first model the minicircle bending prior to any kinks forming. Kinking is the phenomenon that explains deviations from WLC, so prekinking WLC applies for modeling internal energies of the chain. The external energy balancing conformational energy is given by the extensional flow potential. To make the problem tractable, we assume that the DNA adopts the idealized racetrack shape shown in the inset of Figure 2(b). This enables a straightforward evaluation of bending and flow potential energy as a function of the conformation. When we solve for the conformation r that minimizes total energy, we get the nondimensional form

$$\bar{\mu}(r) = \frac{32\pi^4}{r^3\left[(\pi^2 - 6) + \left(\frac{15}{2} - \pi^2\right)r\right]} \quad (1)$$

Over the physical range $0 < r \leq 1$ we have a one-to-one mapping between a particular r and a particular $\bar{\mu}$. We thus have an analytical equation predicting the shape of a DNA minicircle under a particular extensional strain rate. A derivation of eq 1, including the continuum form of the flow-energy term, is provided in the Supporting Information. We plot this equation alongside simulation data from a range of N, $\dot{\epsilon}$ in Figure 3. The theory is able to predict the deformation of the unkinked minicircles with good quantitative accuracy. However, once the system kinks, the simulations deviate from theory. This is most clearly seen by contrasting the unkinked $N = 300$ bp points that continue to follow the theory against the kinked $N = 200$ bp points that begin to deviate between $\bar{\mu} = 20000$–40000. The model was developed using WLC, and kinks have been identified as a mechanism for deviating from WLC, so this is not unexpected. We also note that the $\bar{\mu}$ at which the minicircles begin to kink is different for each N, so the scaling for flow-induced kinking is not captured by $\bar{\mu}$. A different dimensionless grouping is required to fully understand how kinking scales.

https://doi.org/10.1021/acsmacrolett.6c00246
ACS Macro Lett. XXXX, XXX, XXX−XXX

Downloaded from http://pubs.acs.org/amlccd/article-pdf/doi/10.1021/acsmacrolett.6c00246/6627675/acsmacrolett.6c00246.pdf by MASSACHUSETTS INST OF TECHNOLOGY user on 31 July 2026

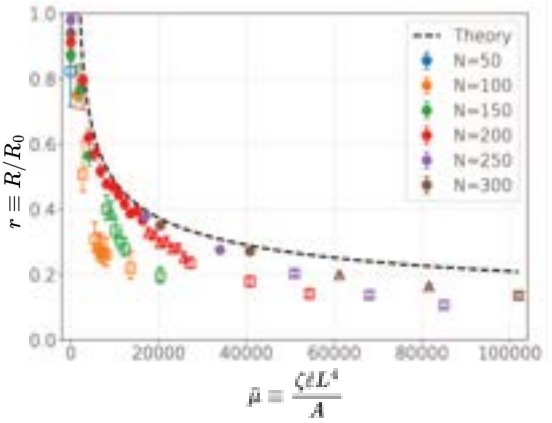

Figure 3. A plot of r against $\bar{\mu}$ for N = 50−300 bp. The analytical prediction for unkinked chains is plotted as a dashed black line. Unkinked minicircles are denoted by filled markers. One kink is indicated by unfilled triangles. Two kinks are indicated by unfilled squares. Error bars show standard deviation.

To characterize the onset of kinking, we return to our model. DNA minicircles in static conditions (no flow) consistently form kinks when they are made small enough. For our DNA minicircles in flow, we assume the existence of a critical curvature κ^* for the semicircle caps beyond which the system kinks. For a racetrack at that curvature, we have

$$\bar{\mu}_{\text{kink}}(L, \kappa^*) = \frac{2\pi}{\frac{\pi^2 - 6}{2} + \frac{\pi\left(\frac{15}{2} - \pi^2\right)}{\kappa^* L}} \tag{2}$$

where $\bar{\mu}_{\text{kink}} \equiv \frac{\zeta \dot{\epsilon} L}{A\kappa^{*3}}$ is a dimensionless parameter predicting the onset of kinking. This $\bar{\mu}_{\text{kink}}$ is the dimensionless balance that results when the racetrack deformation model is evaluated at the local critical curvature for kinking, κ^*. Compared to the elasto-viscous number, it reduces the dependence on minicircle length by three powers and replaces it with a cubic dependence on the critical radius of curvature, $(1/\kappa^*)^3$.

In Figure 4(c), points at different N are plotted for a range of $\bar{\mu}_{\text{kink}}$ and filled if the system displays kinking. To be specific, we track the fraction of time the minicircles spend kinked, and if that fraction is above 0.03, we mark that the system has kinked. The nonzero threshold avoids classifying transient noise as kinking. There is no definitive critical curvature at which kinking occurs, so we use a radius of curvature range of 3.5−4.0 nm, corresponding to available data.[15] We invert to get κ^* = 0.25−0.29 nm^{-1}. This range is reflected in the uncertainty shown in the plot. We see that $\bar{\mu}_{\text{kink}}$ roughly captures the scaling behavior of DNA minicircles kinking in elongational flow. Kinking consistently occurs around $O(\bar{\mu}_{\text{kink}}) \sim 1$, indicating our dimensionless grouping effectively captures the transition. We thus anticipate that for fixed material parameters A, κ^* and drag ζ, if our chain length doubled we would expect half the strain rate necessary to induce kinking, but only one 16th the strain rate to achieve a comparable deformation. This extends to increasing chain lengths until alternative mechanisms become relevant, such as excluded volume where the chain may no longer deform because the linear sides of the racetrack are in contact. Because the controlling forcing is $\zeta\dot{\epsilon}$, increasing the effective drag, for example in a more viscous solvent, would also lower the physical strain rate needed to reach the same dimensionless threshold.

The black curve in Figure 4(c) shows eq 2, which overpredicts the flow forcing required to induce kinking for a given N. A major reason is that the theory is based on the mean racetrack shape and therefore does not account for thermal curvature fluctuations. This is illustrated in Figure 4(a). The racetrack semicircle in black represents the mean racetrack cap curvature, whereas the real contour fluctuates about that mean, as shown schematically in orange. The corresponding curvature profiles in Figure 4(b) show that the semicircle has constant curvature, while thermal fluctuations generate substantial variation and intermittently larger curvature. Because kinking is triggered by localized bending, these fluctuations lower the flow forcing required for kinking to occur.

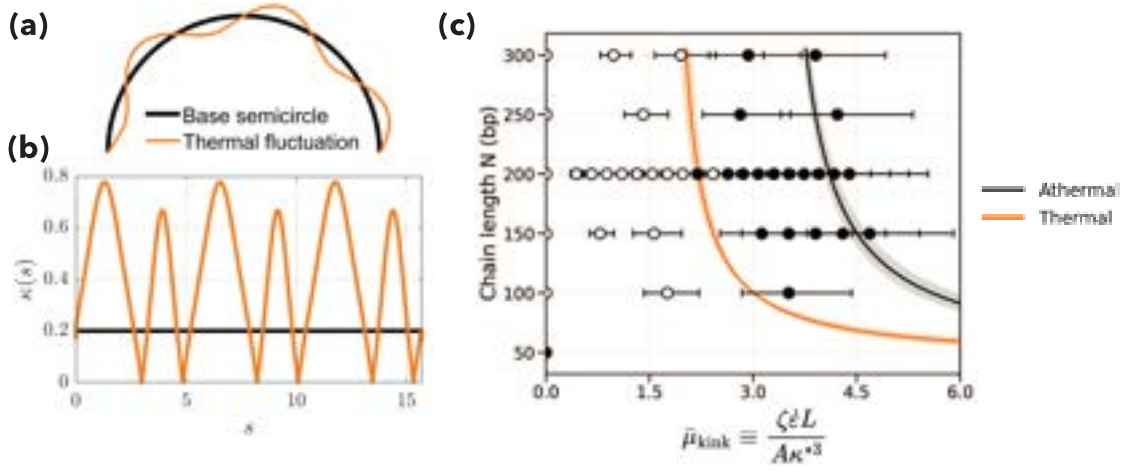

Figure 4. (a) Schematic of a semicircular cap (black) and a thermally fluctuating contour (orange). (b) The curvature $\kappa(s)$ along the corresponding arcs. The semicircle has constant curvature, whereas the fluctuating contour exhibits substantial variation. (c) Kinking phase plot as a function of the dimensionless kinking number $\bar{\mu}_{\text{kink}}$ and chain length N. Filled markers denote minicircles that were kinked above 3% of the time in simulation, and open markers denote below 3%. Error bars on the points and the shaded regions about the athermal and thermal theory curves reflect the estimated critical curvature range κ^* = 0.25−0.29 nm^{-1}.[15] The black curve is the athermal prediction from eq 2. The orange curve includes a thermal correction based on 2D WLC curvature fluctuations, with the threshold fitted to the leftmost kinked point excluding N = 50.[42,43]

https://doi.org/10.1021/acsmacrolett.6c00246
ACS Macro Lett. XXXX, XXX, XXX−XXX

Downloaded from http://pubs.acs.org/amlccd/article-pdf/doi/10.1021/acsmacrolett.6c00246/6627675/acsmacrolett.6c00246.pdf by MASSACHUSETTS INST OF TECHNOLOGY user on 31 July 2026

Prior to kinking the minicircle remains well-described by WLC elasticity, so we model these fluctuations using the WLC curvature distribution. The worm-like chain follows

$$P[\theta(s)] \propto \exp\left[-\frac{l_p}{2}\int_0^L \mathrm{d}s\left(\frac{\mathrm{d}\theta}{\mathrm{d}s}\right)^2\right] \tag{3}$$

for a continuous chain of length L.[44] Over a short interval Δs_c with approximately constant curvature,

$$\frac{l_p}{2}\int_{\Delta s_c} \mathrm{d}s\left(\frac{\mathrm{d}\theta}{\mathrm{d}s}\right)^2 \approx \frac{l_p \Delta s_c}{2}\kappa_s^2 \tag{4}$$

Upon normalization, the curvature of a 2D WLC is therefore Gaussian distributed,

$$P_{2D}(\kappa) = \sqrt{\frac{l_p \Delta s_c}{2\pi}}\exp\left(-\frac{l_p \Delta s_c \kappa^2}{2}\right) \tag{5}$$

with standard deviation $\delta\kappa \sim (l_p \Delta s_c)^{-1/2}$. We take $\Delta s_c \approx 3a$, since three base pairs are required to define the local curvature associated with the base-pair-melting mechanism used here to identify kinks.

We model thermal fluctuations phenomenologically by allowing kinking to occur once the mean cap curvature approaches the critical curvature to within a range of $n_\sigma \delta\kappa$, where n_σ is fit to the data. We determine n_σ by increasing it until the thermal curve reaches the leftmost kinked data point, excluding the $N = 50$ minicircle, which lies outside the regime where the racetrack theory applies. This choice reflects the fact that, in finite-duration simulations, observed kinking is a more reliable marker of threshold crossing than the absence of kinking. At $T = 300$ K, this gives $n_\sigma = 0.356$, and the corresponding orange curve is plotted in Figure 4(c). This quantitative result gives a prediction for the onset of kinking under thermal fluctuations while preserving the connection to the racetrack theory.

Accounting for thermal fluctuations shifts the predicted kinking threshold to lower forcing, as expected. The remaining breakdown at $N = 50$ is also expected: eq 2 assumes that the minicircle first adopts a racetrack shape and only then kinks, whereas the shortest minicircles kink even without flow. This can be seen from the $\kappa^* L$ term in eq 2: since $\pi\left(\frac{15}{2} - \pi^2\right) < 0$, decreasing L drives the predicted threshold to increasingly high values. Physically, the critical-curvature range $\kappa^* = 0.25-0.29$ nm^{-1} corresponds to minicircles of roughly 64−74 bp, so sufficiently short chains are already beyond the regime where the racetrack picture applies. For longer chains, however, the theory preserves the scaling result that the onset of kinking is governed by a balance proportional to $\zeta\dot{\epsilon}L$, so that, all else fixed, a chain twice as long is expected to kink at roughly half the strain rate.

In this work, we showed that uniaxial elongational flow reshapes DNA minicircles by localizing curvature toward the minicircle extrema along the extensional axis, leading to racetrack-like deformation before the onset of kinking. The unkinked response is captured by a racetrack model combining worm-like chain bending with the extensional flow potential, and the simulation data collapse across chain lengths when expressed in terms of the elasto-viscous number $\bar{\mu} = \zeta\dot{\epsilon}L^4/A$. We found that deformation and flow-induced kinking are controlled by different dimensionless balances. Kinking begins when the localized cap curvature approaches a critical value κ^*, which leads to the kinking number $\bar{\mu}_{\mathrm{kink}} = \zeta\dot{\epsilon}L/(A\kappa^{*3})$. For fixed drag, bending stiffness, and critical curvature, this implies that the strain rate required to induce kinking scales with $1/L$, whereas the strain rate to achieve comparable deformation scales with $1/L^4$. The chain length affects global deformation and local structural transition in different ways. Accounting for thermal curvature fluctuations lowers the predicted kinking threshold, bringing the model closer to simulations. Future work could extend these results to other forms of nonuniform forcing, including flow fields with different symmetries and contact-mediated forces in confined geometries such as nanopores, where the deformation pathways may differ from the uniaxial extensional case studied here. These ideas could also be applied to more complex structures, such as DNA catenanes and mechanically interlocked materials.[45,46]

EXPERIMENTAL SECTION

DNA minicircles were modeled with the oxDNA2 coarse-grained representation. Initial conformations were generated as uniformly discretized rings of N base pairs, relaxed and equilibrated in standalone oxDNA at 300 K, and then converted to LAMMPS input using tacoxDNA. Flow simulations were carried out with the oxDNA2 LAMMPS implementation at 300 K and 0.1 M monovalent salt using Langevin dynamics and time step $\Delta t = 0.001$ in oxDNA LAMMPS reduced units, corresponding to approximately 1.71 fs per integration step. Salt-screened electrostatics were treated through the Debye−Hückel term in oxDNA2. Uniaxial extensional flow was imposed through a position-dependent body force proportional to displacement from the center of mass, corresponding to the quadratic uniaxial extensional flow potential. Trajectories were run until steady-state was reached and only poststeady-state frames were used for deformation and kink analysis. Simulations used mixed sequences generated by assigning each base-pair position to be GC with probability 0.41, chosen to approximate human genomic GC content. Homogeneous AT and GC 200 bp minicircles were simulated separately to assess the effect of sequence on deformation and kinking behavior. The specific mixed sequences, sequence-dependence results, additional simulation details, physical interpretations, fitting procedures, and kink-detection criteria are provided in the Supporting Information.

ASSOCIATED CONTENT

Supporting Information

The Supporting Information is available free of charge at https://pubs.acs.org/doi/10.1021/acsmacrolett.6c00246.

Details of simulation protocol, data processing, racetrack fitting, theory derivation, curvature in simulations, and sequence dependence (PDF)

Supporting movies of representative 200 bp minicircles at no flow and at the highest forcing in Fig. 2(a), $\zeta\dot{\epsilon} = 5.27 \times 10^5\,\mathrm{N/m^{-2}}$. Movies are time-compressed for visualization (ZIP)

AUTHOR INFORMATION

Corresponding Author

Patrick S. Doyle − *Department of Chemical Engineering, Massachusetts Institute of Technology, Cambridge, Massachusetts 02139, United States;* orcid.org/0000-0003-2147-9172; Email: pdoyle@mit.edu

Author

Richard B. Huang − *Department of Chemical Engineering, Massachusetts Institute of Technology, Cambridge, Massachusetts 02139, United States*

https://doi.org/10.1021/acsmacrolett.6c00246
ACS Macro Lett. XXXX, XXX, XXX−XXX

Downloaded from http://pubs.acs.org/amlccd/article-pdf/doi/10.1021/acsmacrolett.6c00246/6627656/acsmacrolett.6c00246.pdf by MASSACHUSETTS INST OF TECHNOLOGY user on 31 July 2026

Complete contact information is available at: https://pubs.acs.org/10.1021/acsmacrolett.6c00246

Notes

The authors declare no competing financial interest.

■ ACKNOWLEDGMENTS

The authors acknowledge the MIT SuperCloud and Lincoln Laboratory Supercomputing Center for providing HPC resources that have contributed to the research results reported within this paper (Reuther et al. Interactive supercomputing on 40000 cores for machine learning and data analysis. 2018 IEEE High Performance extreme Computing Conference (HPEC). 2018; p 1−6). This work also used ACES at Texas A&M University's High Performance Research Computing through allocation BIO250226 from the Advanced Cyberinfrastructure Coordination Ecosystem: Services & Support (ACCESS) program, which is supported by U.S. National Science Foundation Grant Nos. 2138259, 2138286, 2138307, 2137603, and 2138296 (Boerner et al. ACCESS: Advancing Innovation: NSF's Advanced Cyberinfrastructure Coordination Ecosystem: Services & Support. Practice and Experience in Advanced Research Computing (PEARC '23). 2023). This material is based upon work supported by the National Science Foundation Graduate Research Fellowship Program under Grant No. 2141064. P.S.D. acknowledges support from the National Science Foundation grant CBET-2510937. The authors thank Dr. Arjav Shah for helpful discussions and early assistance with adapting published oxDNA/LAMMPS simulation workflows during the initial stages of this work.

■ REFERENCES

(1) Schroeder, C. M. Single polymer dynamics for molecular rheology. *J. Rheol.* **2018**, *62*, 371−403.
(2) Dey, S.; Fan, C.; Gothelf, K. V.; Li, J.; Lin, C.; Liu, L.; Liu, N.; Nijenhuis, M. A. D.; Saccà, B.; Simmel, F. C.; Yan, H.; Zhan, P. DNA origami. *Nature Reviews Methods Primers* **2021**, *1*, 13.
(3) Ji, J.; Karna, D.; Mao, H. DNA origami nano-mechanics. *Chem. Soc. Rev.* **2021**, *50*, 11966−11978.
(4) Shah, A.; Lee, X. K.; Li, K.; Knappe, G. A.; Bathe, M.; Barbastathis, G.; Doyle, P. S. Interpretable Deep Learning for Single-Molecule Nanopore Fingerprinting Using Physics-Guided Preprocessing. *ACS Sensors* **2026**, *11*, 3828−3839.
(5) Confederat, S.; Sandei, I.; Mohanan, G.; Wälti, C.; Actis, P. Nanopore fingerprinting of supramolecular DNA nanostructures. *Biophys. J.* **2022**, *121*, 4882−4891.
(6) Zhu, L.; Zhang, Z.; Liu, Q. Deformation-mediated translocation of DNA origami nanoplates through a narrow solid-state nanopore. *Analytical chemistry* **2020**, *92*, 13238−13245.
(7) Shrestha, P.; Emura, T.; Koirala, D.; Cui, Y.; Hidaka, K.; Maximuck, W. J.; Endo, M.; Sugiyama, H.; Mao, H. Mechanical properties of DNA origami nanoassemblies are determined by Holliday junction mechanophores. *Nucleic acids research* **2016**, *44*, 6574−6582.
(8) De Gennes, P. Coil-stretch transition of dilute flexible polymers under ultrahigh velocity gradients. *J. Chem. Phys.* **1974**, *60*, 5030−5042.
(9) Perkins, T. T.; Smith, D. E.; Chu, S. Single polymer dynamics in an elongational flow. *Science* **1997**, *276*, 2016−2021.
(10) De Gennes, P. Molecular individualism. *Science* **1997**, *276*, 1999−2000.
(11) Hsieh, C.-C.; Larson, R. G. Prediction of coil-stretch hysteresis for dilute polystyrene molecules in extensional flow. *J. Rheol.* **2005**, *49*, 1081−1089.
(12) Schroeder, C. M.; Babcock, H. P.; Shaqfeh, E. S.; Chu, S. Observation of polymer conformation hysteresis in extensional flow. *Science* **2003**, *301*, 1515−1519.
(13) Li, Y.; Hsiao, K.-W.; Brockman, C. A.; Yates, D. Y.; Robertson-Anderson, R. M.; Kornfield, J. A.; San Francisco, M. J.; Schroeder, C. M.; McKenna, G. B. When ends meet: Circular DNA stretches differently in elongational flows. *Macromolecules* **2015**, *48*, 5997−6001.
(14) Yoo, J.; Park, S.; Maffeo, C.; Ha, T.; Aksimentiev, A. DNA sequence and methylation prescribe the inside-out conformational dynamics and bending energetics of DNA minicircles. *Nucleic acids research* **2021**, *49*, 11459−11475.
(15) Vologodskii, A.; Frank-Kamenetskii, M. D. Strong bending of the DNA double helix. *Nucleic Acids Research* **2013**, *41*, 6785−6792.
(16) Harrison, R. M.; Romano, F.; Ouldridge, T. E.; Louis, A. A.; Doye, J. P. Identifying physical causes of apparent enhanced cyclization of short DNA molecules with a coarse-grained model. *J. Chem. Theory Comput.* **2019**, *15*, 4660−4672.
(17) Lankaš, F.; Lavery, R.; Maddocks, J. H. Kinking occurs during molecular dynamics simulations of small DNA minicircles. *Structure* **2006**, *14*, 1527−1534.
(18) Ouldridge, T. E. *Coarse-grained modelling of DNA and DNA self-assembly*; Springer Science & Business Media, 2012.
(19) Snodin, B. E. K.; Randisi, F.; Mosayebi, M.; Sulc, P.; Schreck, J. S.; Romano, F.; Ouldridge, T. E.; Tsukanov, R.; Nir, E.; Louis, A. A.; Doye, J. P. K. Introducing improved structural properties and salt dependence into a coarse-grained model of DNA. *J. Chem. Phys.* **2015**, *142*, 234901.
(20) Sengar, A.; Ouldridge, T. E.; Henrich, O.; Rovigatti, L.; Šulc, P. A primer on the oxDNA model of DNA: when to use it, how to simulate it and how to interpret the results. *Frontiers in Molecular Biosciences* **2021**, *8*, No. 693710.
(21) Park, G.; Cho, M. K.; Jung, Y. Sequence-dependent kink formation in short DNA loops: theory and molecular dynamics simulations. *J. Chem. Theory Comput.* **2021**, *17*, 1308−1317.
(22) Romano, F.; Chakraborty, D.; Doye, J. P. K.; Ouldridge, T. E.; Louis, A. A. Coarse-grained simulations of DNA overstretching. *J. Chem. Phys.* **2013**, *138*, 085101.
(23) Mosayebi, M.; Louis, A. A.; Doye, J. P. K.; Ouldridge, T. E. Force-Induced Rupture of a DNA Duplex: From Fundamentals to Force Sensors. *ACS Nano* **2015**, *9*, 11993−12003.
(24) Engel, M. C.; Smith, D. M.; Jobst, M. A.; Sajfutdinow, M.; Liedl, T.; Romano, F.; Rovigatti, L.; Louis, A. A.; Doye, J. P. Force-induced unravelling of DNA origami. *ACS Nano* **2018**, *12*, 6734−6747.
(25) Suma, A.; Micheletti, C. Pore translocation of knotted DNA rings. *Proc. Natl. Acad. Sci. U.S.A.* **2017**, *114*, E2991−E2997.
(26) Suma, A.; Micheletti, C. Unzipping of knotted DNA via nanopore translocation. *QRB Discovery* **2025**, *6*, e4.
(27) Henrich, O.; Gutiérrez Fosado, Y. A.; Curk, T.; Ouldridge, T. E. Coarse-grained simulation of DNA using LAMMPS: An implementation of the oxDNA model and its applications. *Eur. Phys. J. E* **2018**, *41*, 1−16.
(28) Poppleton, E.; Bohlin, J.; Matthies, M.; Sharma, S.; Zhang, F.; Šulc, P. Design, optimization and analysis of large DNA and RNA nanostructures through interactive visualization, editing and molecular simulation. *Nucleic acids research* **2020**, *48*, e72−e72.
(29) Stukowski, A. Visualization and analysis of atomistic simulation data with OVITO−the Open Visualization Tool. *Modell. Simul. Mater. Sci. Eng.* **2010**, *18*, No. 015012.
(30) Ouldridge, T. E.; Hoare, R. L.; Louis, A. A.; Doye, J. P.; Bath, J.; Turberfield, A. J. Optimizing DNA nanotechnology through coarse-grained modeling: a two-footed DNA walker. *ACS Nano* **2013**, *7*, 2479−2490.
(31) Liu, Y.; Chakrabarti, B.; Saintillan, D.; Lindner, A.; Du Roure, O. Morphological transitions of elastic filaments in shear flow. *Proc. Natl. Acad. Sci. U. S. A.* **2018**, *115*, 9438−9443.

Downloaded from http://pubs.acs.org/amlccd/article-pdf/doi/10.1021/acsmacrolett.6c00246/6276756/acsmacrolett.6c00246.pdf by MASSACHUSETTS INST OF TECHNOLOGY user on 31 July 2026

(32) Żuk, P. J.; Słowicka, A. M.; Ekiel-Jeżewska, M. L.; Stone, H. A. Universal features of the shape of elastic fibres in shear flow. *J. Fluid Mech.* **2021**, *914*, A31.
(33) Marko, J. F.; Siggia, E. D. Stretching dna. *Macromolecules* **1995**, *28*, 8759−8770.
(34) Kratky, O.; Porod, G. Röntgenuntersuchung gelöster Fadenmoleküle. *Recueil des Travaux Chimiques des Pays-Bas* **1949**, *68*, 1106−1122.
(35) Cloutier, T. E.; Widom, J. Spontaneous sharp bending of double-stranded DNA. *Mol. Cell* **2004**, *14*, 355−362.
(36) Wiggins, P. A.; van der Heijden, T.; Moreno-Herrero, F.; Spakowitz, A.; Phillips, R.; Widom, J.; Dekker, C.; Nelson, P. C. High flexibility of DNA on short length scales probed by atomic force microscopy. *Nat. Nanotechnol.* **2006**, *1*, 137−141.
(37) Du, Q.; Kotlyar, A.; Vologodskii, A. Kinking the double helix by bending deformation. *Nucleic acids research* **2008**, *36*, 1120−1128.
(38) Le, T. T.; Kim, H. D. Probing the elastic limit of DNA bending. *Nucleic acids research* **2014**, *42*, 10786−10794.
(39) Zheng, X.; Vologodskii, A. Theoretical analysis of disruptions in DNA minicircles. *Biophysical journal* **2009**, *96*, 1341−1349.
(40) Vafabakhsh, R.; Ha, T. Extreme bendability of DNA less than 100 base pairs long revealed by single-molecule cyclization. *Science* **2012**, *337*, 1097−1101.
(41) Crick, F.; Klug, A. Kinky helix. *Nature* **1975**, *255*, 530.
(42) Smith, M. B.; Li, H.; Shen, T.; Huang, X.; Yusuf, E.; Vavylonis, D. Segmentation and tracking of cytoskeletal filaments using open active contours. *Cytoskeleton* **2010**, *67*, 693−705.
(43) Rappaport, S. M.; Medalion, S.; Rabin, Y. Curvature distribution of worm-like chains in two and three dimensions. *arXiv:0801.3183 [cond-mat.soft]* **2008**, na.
(44) Marantan, A.; Mahadevan, L. Mechanics and statistics of the worm-like chain. *American Journal of Physics* **2018**, *86*, 86−94.
(45) Sakai, Y.; Wilkens, G. D.; Wolski, K.; Zapotoczny, S.; Heddle, J. G. Topogami: topologically linked DNA origami. *ACS Nanoscience Au* **2022**, *2*, 57−63.
(46) Peil, A.; Zhan, P.; Liu, N. DNA origami catenanes templated by gold nanoparticles. *Small* **2020**, *16*, 1905987.

Downloaded from http://pubs.acs.org/amlccd/article-pdf/doi/10.1021/acsmacrolett.6c00246/6627656/acsmacrolett.6c00246.pdf by MASSACHUSETTS INST OF TECHNOLOGY user on 31 July 2026

https://doi.org/10.1021/acsmacrolett.6c00246
ACS Macro Lett. XXXX, XXX, XXX−XXX